Int. J. Electrochem. Sci., 15 **(2020)** 6052 – 6059, doi: 10.20964/2020.07.64

International Journal of
ELECTROCHEMICAL
SCIENCE
www.electrochemsci.org

Synthesis and Properties of Halloysite Templated Tubular MoS_2 as Cathode Material for Rechargeable Aqueous Zn-ion Batteries

Yang Yang[1,a], *Xiuyun Chuan*[1,*], *Jianzhuo Li*[1,a], *Fangfang Liu*[1], *Aijun Li*[1,2]

[1] Key Laboratory of Orogenis Belts and Crustal Evolution, School of Earth and Space Sciences, Peking University, Beijing 100871, China
[2] Beijing Golden Feather Energy Technology Co., Ltd., Beijing 100095, China
[*]E-mail: xychuan@pku.edu.cn
[a]Author contributes equal to this work

Received: 3 March 2020 / *Accepted:* 26 April 2020 / *Published:* 10 June 2020

Aqueous Zn-ion battery (ZIB) is recognized as one of the most promising candidates for large-scale energy storage due to its unique properties of excellent safety, cost effectiveness and environmental benignity. However, the application of ZIB is hampered by the restricted availability of suitable cathode materials. In this work, porous tubular MoS_2 was prepared by template-assisted thermal decomposition, in which $(NH_4)_2MoS_4$ was utilized as a precursor and natural halloysite as a template. As a promising cathode material for ZIB, the prepared MoS_2 exhibited a good specific capacity of 146.2 mAh g^{-1} at 0.2 A g^{-1} and excellent cycling performance with 74.0% capacity retention after 800 cycles. Furthermore, the proposed MoS_2 demonstrated a great rate capability even at 1 A g^{-1}. This work provides a promising cathode material for ZIBs, and opens up new possibilities for its future application in renewable energy storage.

Keywords: MoS_2; thermal decomposition; halloysite template; cathode; aqueous zinc ion battery.

1. INTRODUCTION

Over the last few decades, Li-ion battery (LIB) has been widely applied in electric vehicles and electronic devices because of its excellent energy density and long life span. However, the high cost, resource shortage and safety issues of Li impede the application of LIB in large-scale energy storage [1-3]. As an alternative, aqueous rechargeable batteries may exhibit a more competitive performance than LIB, due to their unique advantages of good safety, cost effectiveness and environmental benignity [4]. In particular, rechargeable aqueous Zn-ion battery (ZIB) is attractive due to the extraordinary features of Zn, such as multivalent charge transfer, high theoretic capacity (825 mAh g^{-1}), low reduction potential (−0.76 V) and environmental benignity [5-7]. Unfortunately, the cathode materials that enable the

reversible intercalation/deintercalation of zinc ion for ZIB are relatively limited. Several cathode materials, such as MnO_2 [8], Mn_2O_3 [9], Mn_3O_4 [10], VS_2 [11], and Prussian blue [12-13] have been explored thus far. However, all of them demonstrate limited specific capacity and poor cycling performance. Therefore, it is of great significance to develop new electrode materials for ZIB.

Structurally analogous to graphite, MoS_2 is comprised of 1 Mo layer sandwiched between 2 S layers, resulting in S-Mo-S stacks held together by weak (van der Waals) forces with an interlayer spacing of 0.65 nm [14-15]. Owing to its layer structure, the diffusion and transportation of ions in MoS_2 are more rapidly than in oxides [16]. In recent years, MoS_2 has been demonstrated as a prospective cathode material for ZIB. Zhang et al. [17] synthesized a three-dimensional flower-like MoS_2 that displays a specific discharge capacity of 96.9 mAh g^{-1} at 0.1 A g^{-1}. Xu et al. [18] prepared defect-rich MoS_2 nanosheet-like materials that can insert/extract a great amount of Zn^{2+} ions and display an excellent reversible capacity of 135 mAh g^{-1} at 0.1 A g^{-1}. Li et al. [19] integrated vertically aligned MoS_2 nanosheets onto carbon fiber cloth, and the as-fabricated Zn/MoS_2 batteries demonstrated an outstanding specific capacity of 202.6 mAh g^{-1} at 0.1 A g^{-1}, good cycling performance, and excellent rate capability. Liang et al. [20] developed a flower-like MoS_2 with efficient Zn^{2+} diffusivity via simple interlayer spacing and hydrophilic surface modification, and a high Zn^{2+} storage capacity of 232 mAh g^{-1} at 0.1 A g^{-1} was obtained. However, at present, the synthesis of MoS_2 with excellent zinc storage property has been restricted to the conventional hydrothermal methods that suffered from many inferiorities such as high cost, complicated experimental process, low production efficiency and small scale production.

In this work, for the first time, we prepared porous tubular MoS_2 through the decomposition of $(NH_4)_2MoS_4$, and controlled the micromorphology of the product by using natural halloysite as a template. As a result, the as-prepared tubular MoS_2 was shown to be a potential cathode material for ZIB, by displaying a good discharge capacity of 146.2 mAh g^{-1} at 0.2 A g^{-1} with 74.0% capacity retention after 800 cycles. This work provides a new cathode for high performance ZIBs and opens up new possibilities for its future application in large-scale energy storage.

2. EXPERIMENTAL

2.1 Materials preparation

Approximately 0.25 g of ammonium thiomolybdate ($(NH_4)_2MoS_4$, 99%) was added into 10 mL dimethylformamide (DMF, 99%) and then mixed with 5.0 g high-purity halloysite (Yuan Xin Nano Technology Co., Ltd.). The resulting mixture was stirred under vacuum for 30 minutes and dried at 90 ^oC. Then, the obtained product was washed with DMF to remove any residue on the surface of the template. After annealing at 400 ^oC for 2 h under argon flow, the halloysite template was abolished by submerging in 1 mol/L HF/HCl solution for 12 h. The sample was obtained by washing with water and alcohol, followed by additional drying at 90 ^oC in a vacuum oven.

2.2. Characterizations

X-ray diffraction (XRD) pattern was determined by using a Rigaku D/MAX-2400 diffractometer with Cu-K*a* radiation (λ = 0.154056 nm). Raman spectra were recorded at 532 nm excitation using a Ricro-Raman-1000 micro spectrometer (Renishaw, UK). X-ray photoelectron spectroscopy (XPS) analysis was performed by an AXIS SUPRA (Kratos) with Al-Kα radiation. Scanning electron microscopy (SEM) micrographs were obtained using a Nova Nano SEM 430 field emission microscope (FEI, OR, USA). Transmission electron microscope (TEM) images were captured using a Tecnai F30 field emission gun-TEM (FEI, USA). Energy-dispersive X-ray spectroscopy (EDS) was used to characterize the elemental distribution of each sample. Nitrogen adsorption-desorption isotherms at 77.3 K were assessed by a Micromeritics ASAP 2020 system, in order to determine the specific pore volume and surface area.

2.3. Electrochemical measurements

To prepare a cathode slurry, the as-prepared MoS_2, carbon black and polyvinylidene difluoride were mixed in 1-methyl-2-pyrrolidone at a weight ratio of 7:2:1. Then, the resulting slurry was coated onto a graphite sheet and dried at 80 °C under vacuum for 24 h. The mass loading was about 1.0 mg cm^{-2}. Coin cells (type CR2032) were assembled with 3.0 M zinc trifluoromethanesulfonate ($Zn(CF_3SO_3)_2$) solution, glass fiber and zinc foil as the electrolyte, separator and anode, respectively. Galvanostatic charge/discharge measurement was carried out using a LAND-CT2001A battery test system and cyclic voltammetry (CV) analyse was conducted on a CHI660E electrochemical workstation within 0.25-1.25 V versus Zn/Zn^{2+}.

3. RESULTS AND DISCUSSION

As shown in Fig. 1, SEM and TEM were carried out to examine the morphological characteristics of the template and as-prepared MoS_2. The halloysite crystals exhibited a tubular structure with dimensions of approximately 20 nm in inner diameter and 1 μm in length (Fig. 1a). Similar to the morphology of halloysite template, most of the resultant MoS_2 displayed a tubular-like morphology (Fig. 1b and 1c). In agreement with the above-described SEM observations, the TEM images (Fig. 1d and 1e) clearly demonstrated that the hollow tubular structure and outer diameter of MoS_2 nanotube were consistent with the inner diameter of the template, suggesting the as-prepared MoS_2 perfectly inherits the template's morphology. Apart from such tubular-like microscopic features, sheet-like MoS_2 feature was observed in the resultant MoS_2, which might be attributed to the breakage of MoS_2 nanotubes during template removal or ultrasonic treatment [21-22]. High-resolution TEM images of the MoS_2 nanotube clearly showed that MoS_2 exhibited a layer-staked structure with an interlayer spacing of 0.65 nm (Fig. 1e), corresponding to the *d*-spacing of the (002) planes of hexagonal MoS_2 [14]. Fig. 1f shows the EDS analysis of elemental composition in MoS_2. The two elements, Mo and S, were distributed homogeneously and matched well with the selected TEM image (Fig. 1d).

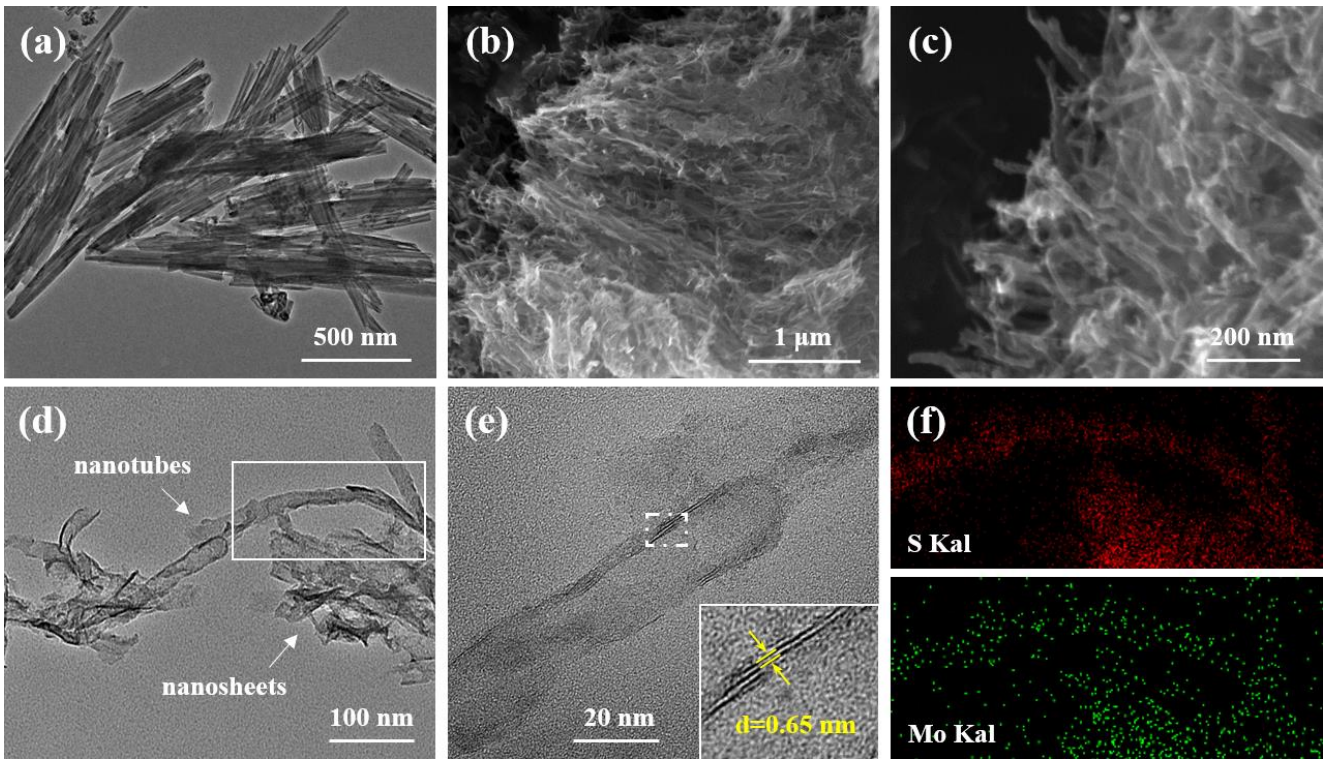

Figure 1. Morphology of prepared tubular MoS_2. (a) TEM image of halloysite template, (b, c) SEM images of tubular MoS_2, (d) TEM and (e) HRTEM images of tubular MoS_2, and (f) elemental distribution scanning of the selected region in (d).

The composition and phase purity of the as-prepared MoS_2 were examined further. The XRD patterns of MoS_2 are demonstrated in Fig. 2a. Notably, all diffraction peaks were well matched with the hexagonal phase of MoS_2 (JCPDS No.37-1492) and no impurity peak was observed, indicating the high purity of the products. The Raman spectra are presented in Fig. 2b, in which two characteristic bands were detected at 381.8 cm^{-1} and 406.9 cm^{-1}, corresponding to the in-plane E^1_{2g} vibration of Mo-S and out-of-plane A_{1g} vibration of MoS_2, respectively [23]. The existence of Mo and S in the prepared materials was further verified by XPS spectra. As shown in Fig. 2c-e, two peaks at 229.0 and 232.5 eV were assigned to Mo^{4+} $3d_{5/2}$ and Mo^{4+} $3d_{3/2}$, respectively. The presence of another peak at 235.4 eV was indexed to Mo^{6+} $3d_{3/2}$, which might be attributed to the surface oxidation. The XPS signals of S 2p were found at 162.6 and 163.8 eV, corresponding to S^{2-} $2p_{3/2}$ and S^{2-} $2p_{1/2}$, respectively [24-26]. The results of XRD, Raman and XPS were all in agreement with the data of HRTEM observation, suggesting the hollow tubular MoS_2 nanotubes are successfully prepared. Moreover, the atomic ratio of Mo/S elements was calculated to be 1:1.4, implying the presence of sulfur vacancies or molybdenum interstitials in the MoS_2 nanosheets. This could be an important factor to improve the electrochemical performance of MoS_2 on zinc ions [18]. As presented in Fig. 2f, the products were also characterized by nitrogen adsorption-desorption isotherms. The synthesized MoS_2 possessed a relatively high BET surface area of 72.4 m^2 g^{-1} with 0.27 cm^3 g^{-1} pore volume and the mesopore with approximately 20 nm width could be clearly observed (insert figure in Fig. 2f), which is mainly caused by the hollow tubular structure. The

porous tubular structure was conducive to the infiltration of electrolyte in active materials, enabling the sufficient utilization of MoS_2.

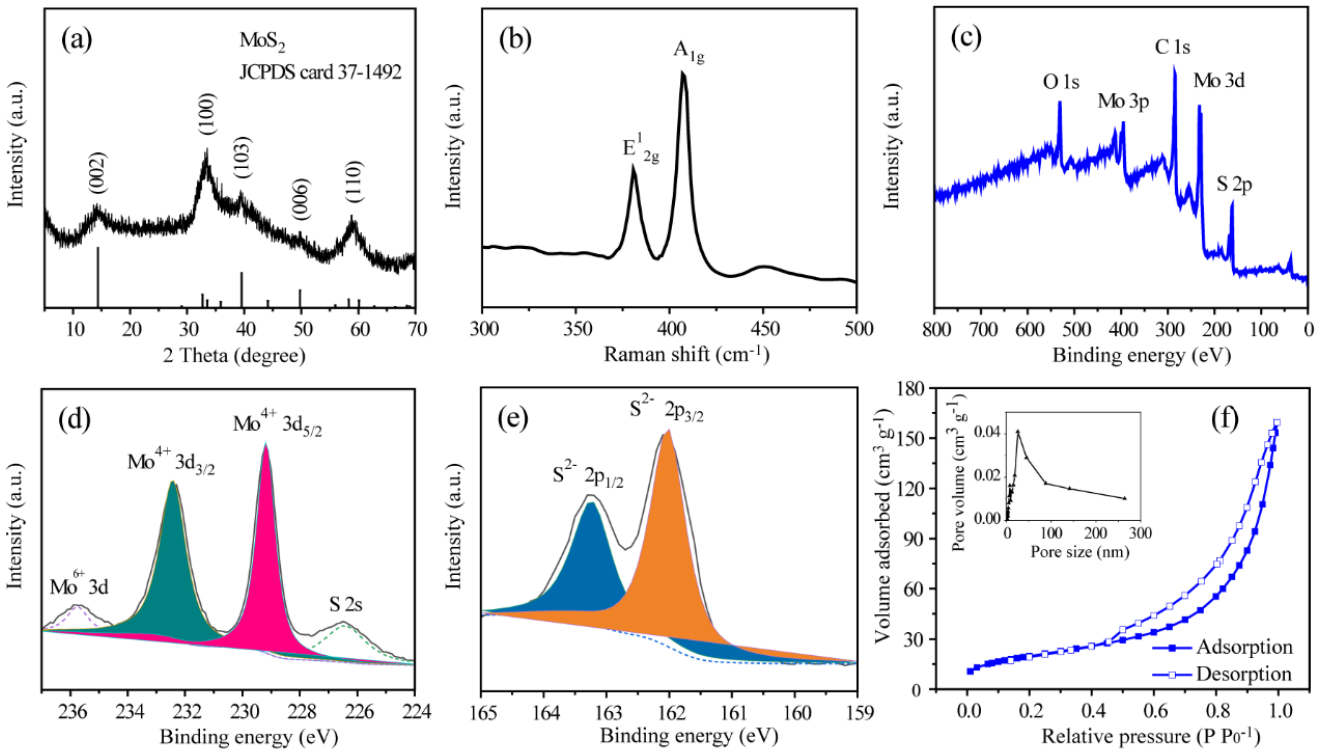

Figure 2. Characterization of prepared MoS_2 sample. (a) XRD patterns and (b) Raman spectra of tubular MoS_2. (c) XPS spectra of tubular MoS_2, and detailed XPS spectra of (d) Mo 3d and S 2s, (e) S 2p. (f) N_2 isotherm curves and pore size distribution (inset) of tubular MoS_2.

To determine the electrochemical properties of the as-prepared MoS_2, a complete battery was built by employing zinc foil as the anode and 3.0 M $Zn(CF_3SO_3)_2$ aqueous solution as the electrolyte. Fig. 3a displays the typical CV curves of the MoS_2 electrode at 1 mV s^{-1} within the potential window of 0.25-1.25 V. Two broad cathodic and anodic peaks positioned at around 0.7 and 1.0 V, respectively, were observed. The reduction peak at 0.7 V was ascribed to the intercalation of Zn^{2+} ions into MoS_2, resulting in the formation of Zn_xMoS_2. Meanwhile, the oxidation peak at 1.0 V was ascribed to the deintercalation of Zn^{2+} [18, 20]. Specifically, the second and third cycles of CV curves were nearly overlapped, implying an excellent reversibility and predominance of the MoS_2 electrode. Fig. 3b shows the CV curves at various scan rates. It was observed that the shape of CV curves remained similar when the scan rates increased from 0.1 to 5.0 mV s^{-1}, indicating the outstanding rate performance and cycling stability of MoS_2. The charge and discharge curves and rate performance of the battery at various current densities are illustrated in Fig. 3c and 3d. The specific capacity and coulombic efficiency at 0.2 A g^{-1} were found to be 133.8 mAh g^{-1} and 96.7%, respectively. The values of specific capacity were decreased with increasing current densities, in which the reversible capacities reached 108.9, 92.9, 86.0 and 82.3 mAh g^{-1} at the current densities of 0.4, 0.6, 0.8 and 1.0 A g^{-1}, respectively. When the current density was

reversed back from 1.0 to 0.2 A g^{-1}, an excellent discharge capacity of 146.2 mAh g^{-1} was observed. Furthermore, the cycling performance of the full cell was assessed at 0.5 A g^{-1}. As shown in Fig. 3e and 3f, although there was a rapid decline from 119.7 to 84.6 mAh g^{-1} in the first 50 cycles, the storage capacities gradually increased and remained stable in the following cycles. After 800 cycles, the product still delivered a discharge capacity of 88.6 mAh g^{-1} with 74.0% capacity retention, indicating a remarkable cycling stability of MoS_2 electrode. The excellent electrochemical performance of the tubular MoS_2 may be ascribed to its unique microstructure. (1) the sulfur vacancies or molybdenum interstitials in the MoS_2 nanosheets can readily accommodate intercalated Zn^{2+} ions, resulting in excellent reversible zinc storage capacity [18]. (2) the porous tubular structure is conducive to the infiltration of electrolyte and the rapid diffusion of ions in active materials, facilitating the electrons transport during the processes of charging and discharging.

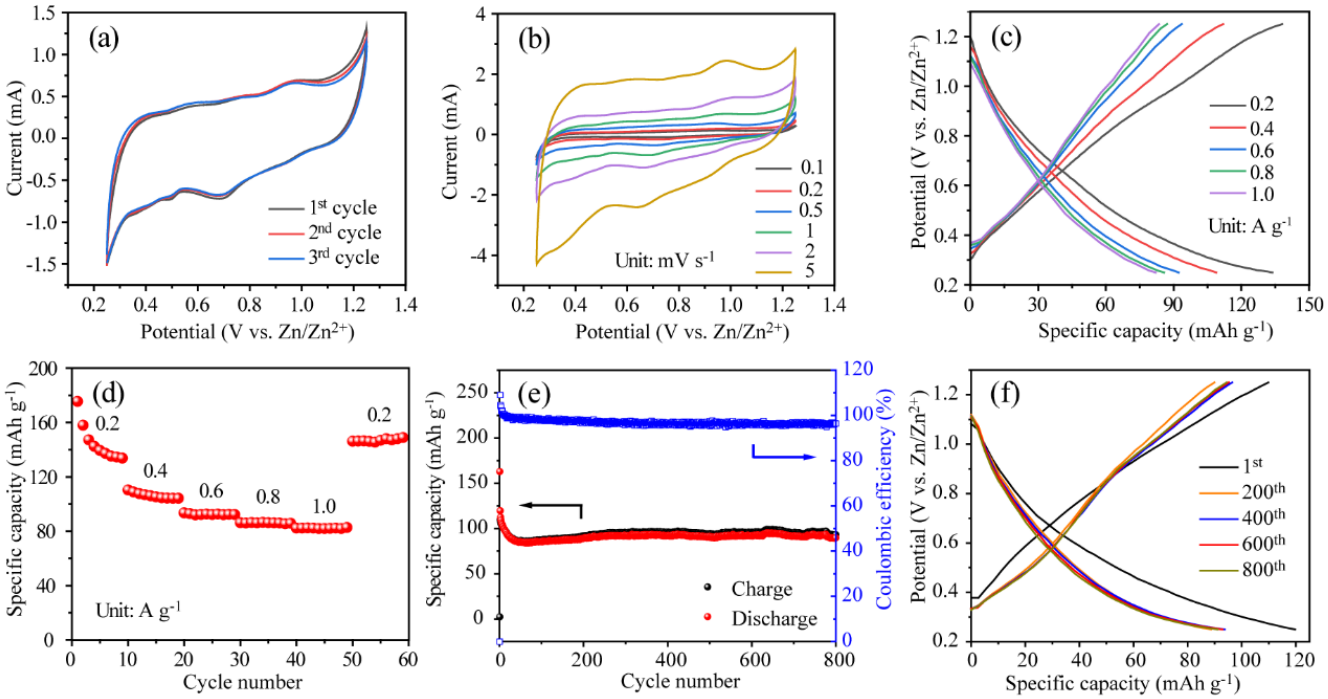

Figure 3. Electrochemical performance of Zn/MoS_2 full cells. (a) The first three CV curves at 1 mV s^{-1} and (b) CV curves at different scan rates of Zn/MoS_2 cell; (c) the charge/discharge curves and (d) rate performance of Zn/MoS_2 cell at different current densities; (e) cycling performance at 0.5 A g^{-1} and (f) the voltage profiles at different cycles.

As per our knowledge, only limited works on MoS_2 as the cathode of ZIB has been reported so far and the synthesis of MoS_2 with excellent zinc storage property has been restricted to the conventional hydrothermal methods. Table 1 shows the comparison of electrochemical performances of various MoS_2 for ZIB applications. Although the performance of MoS_2 prepared by template-assisted thermal decomposition is not so outstanding, it offers a new method for the preparation of MoS_2 with high zinc storage capacity and expands the application of natural mineral materials in ZIB. Therefore, it shows a promising prospect in industrial applications.

Table 1. Comparisons between the as-prepared MoS_2 and other MoS_2 reported previously for ZIB applications

Electrode materials	Method	Capacitance	References
Three-dimensional flower-like MoS_2	Hydrothermal method	96.9 $mAh \cdot g^{-1}$ at 100 $mA \cdot g^{-1}$	[17]
Defect-rich MoS_2 nanosheets	Hydrothermal method	138.6 $mAh \cdot g^{-1}$ at 100 $mA \cdot g^{-1}$	[18]
MoS_2 nanosheets with expanded inter-layer spacing	Hydrothermal method	202.6 $mAh \cdot g^{-1}$ at 100 $mA \cdot g^{-1}$	[19]
MoS_2 nanosheets with oxygen incorporation	Hydrothermal method	232 $mAh \cdot g^{-1}$ at 100 $mA \cdot g^{-1}$	[20]
Tubular MoS_2	Template-assisted thermal decomposition method	146.2 $mAh \cdot g^{-1}$ at 200 $mA \cdot g^{-1}$	This work

4. CONCLUSIONS

In summary, porous tubular MoS_2 was successfully prepared, for the first time, by using $(NH_4)_2MoS_4$ as a precursor and natural halloysite as a template. As a cathode candidate for ZIB, the MoS_2 electrode exhibited a desirable discharge capacity of 146.2 mAh g^{-1} at 0.2 A g^{-1}. In addition, the proposed ZIB had a good capacity reversibility and good long-term cyclic stability. Overall, this work expands the application of natural mineral materials in electrochemical energy storage and opens up new possibilities for the future application of ZIB in large-scale energy storage.

ACKNOWLEDGEMENTS
This work was supported by National Natural Science Foundation of China (51774016) and Test Fund of Peking University (0000012321).

References

1. D. Larcher and J. M. Tarascon, *Nat. Chem.*, 7 (2015) 19.
2. B. G. John and K. Youngsik, *J. Power Sources*, 196 (2011) 6688.
3. B. G. John and K. S. Park, *J. Am. Chem. Soc.*, 135 (2013) 1167.
4. L. Chen, L. Zhang, X. Zhou and Z. Liu, *ChemSusChem*, 7 (2014) 2295.
5. G. Fang, J. Zhou, A. Pan and S. Liang, *ACS Energy Lett.*, 3 (2018) 2480.
6. M. Song, H. Tan, D. Chao and H. J. Fan, *Adv. Funct. Mater.*, 28 (2018) 1802564.
7. P. Yu, Y. Zeng, H. Zhang, M. Yu, Y. Tong and X. Lu, *Small*, 15 (2019) 1804760.
8. F. Mo, H. Li, Z. Pei, G. Liang, L. Ma, Q. Yang, D. Wang, Y. Huang and C. Zhi, *Sci. Bull*, 63 (2018) 1077.
9. B. Jiang, C. Xu, C. Wu, L. Dong, J. Li and F. Kang, *Electrochim. Acta*, 229 (2017) 422.
10. L. Wang, X. Cao, L. Xu, J. Chen and J. Zheng, *ACS Sustainable Chem. Eng.*, 6 (2018) 16055.
11. P. He, M. Yan, G. Zhang, R. Sun, L. Chen, Q. An and L. Mai, *Energy Storage Mater.*, 7 (2017) 1601920.
12. Z. Liu, G. Pulletikurthi and F. Endres, *ACS Appl. Mater. Interfaces*, 8 (2016) 12158.
13. L. Zhang, L. Chen, X. Zhou and Z. Liu, *Adv. Energy Mater.*, 5 (2015) 1400930.

14. Z. He and W. Que, *Appl. Mater. Today*, 3 (2016) 23.
15. Y. Yang, A. Li, X. Cao, F. Liu, S. Cheng and X. Chuan, *RSC Adv.*, 8 (2018) 35672.
16. K.-J. Huang, L. Wang, Y.-J. Liu, H.-B. Wang, Y.-M. Liu and L.-L. Wang, *Electrochim. Acta*, 109 (2013) 587.
17. G. Zhang, L. Hu and B. Zhang, *Mater. Rep.*, 30 (2016) 284.
18. W. Xu, C. Sun, K. Zhao, X. Cheng, S. Rawal, Y. Xu and Y. Wang, *Energy Storage Mater.*, 16 (2019) 527.
19. H. Li, Q. Yang, F. Mo, G. Liang, Z. Liu, Z. Tang, L. Ma, J. Liu, Z. Shi and C. Zhi, *Energy Storage Mater.*, 19 (2019) 94.
20. H. Liang, Z. Cao, F. Ming, W. Zhang, D. H. Anjum, Y. Cui, L. Cavallo and H. N. Alshareef, *Nano Lett.*, 19 (2019) 3199.
21. A. Wang, F. Kang, Z. Huang, Z. Guo and X. Chuan, *Microporous Mesoporous Mater.*, 108 (2008) 318.
22. Z. Huang, A. Wang, F. Kang and X. Chuan, *Mater. Lett.*, 64 (2010) 2444.
23. C. Lee, H. Yan, L. E. Brus, T. F. Heinz, J. Hone and S. Ryu, *ACS Nano*, 4 (2010) 2695.
24. X. Zhou, L. Wan and Y. Guo, *Nanoscale*, 4 (2012) 5868.
25. Y. Sun, X. Hu, J. C. Yu, Q. Li, W. Luo, L. Yuan, W. Zhang and Y. Huang, *Energy Environ. Sci.*, 4 (2011) 2870.
26. X. Xiong, W. Luo, X. Hu, C. Chen, L. Qie, D. Hou and Y. Huang, *Sci. Rep.*, 5 (2015) 9254.